miR-637 prevents glioblastoma progression by interrupting ZEB2/WNT/β-catenin cascades

Wei Wang
The First Hospital of China Medical University: The First Affiliated Hospital of China Medical University
Zilong Zhou
The First Hospital of China Medical University: The First Affiliated Hospital of China Medical University
Shuai Han
The First Hospital of China Medical University: The First Affiliated Hospital of China Medical University
Di Wu (windy_wu0802@163.com)
The First Affiliated Hospital of China Medical University https://orcid.org/0000-0002-2594-1072

Research Article

Keywords: miR-637, ZEB2, WNT7A, β-catenin, glioblastoma progression

Posted Date: March 30th, 2021

DOI: https://doi.org/10.21203/rs.3.rs-246383/v1

Abstract

Glioblastomas (GBMs) are the most frequent primary malignancies in the central nervous system. Aberrant activation of WNT/β-catenin signaling pathways is critical for GBM malignancy. However, the regulation of WNT/β-catenin signaling cascades remains unclear. Presently, we observed the increased expression of ZEB2 and decreased expression of miR-637 in GBM. The expression of miR-637 was negatively correlated with expression of ZEB2. miR-637 overexpression overcame the ZEB2-enhanced cell proliferation and G1/S phase transition. In addition, miR-637 suppressed canonical WNT/β-catenin pathways by targeting WNT7A directly. Gain- and loss-of-function experiments in U251 mice demonstrated that miR-637 inhibited cell proliferation and arrested the G1/S phase transition, leading to tumor growth suppression. The collective findings suggest that ZEB2 and WNT/β-catenin cascades merge at miR-637 and the ectopic expression of miR-637 disturbs ZEB2/WNT/β-Catenin-mediated GBM growth. The findings should inform improved β-catenin-targeted therapy against GBM.

Introduction

Gliomas are the most frequent primary malignancies in the central nervous system. According to their histopathological characteristics, gliomas are categorized as grades I, II, III, and IV (glioblastoma, GBM) according to the World Health Organization (WHO) classification for central nervous system tumors (Chen et al. 2017). Histologic criteria are essential for the diagnosis of gliomas. Molecular characteristics have been introduced into the classification system to refine the diagnostic standard, prognostic markers, and the initial options for targeted therapies (Reifenberger et al. 2017). These characteristics include *MGMT* (O6-methylguanine-DNA methyltransferase) promoter methylation, *IDH* (isocitrate dehydrogenase) mutations, chromosome 1p/19q deletion, and *EGFR* (epidermal growth factor receptor) amplification. Particularly, mounting evidence has demonstrated that WNT/β-catenin signaling pathways are frequently hyperactive in GBM and so are a promising therapeutic target against GBM progression (He et al. 2019). However, the dysregulation of WNT/β-catenin in GBM has not been fully investigated.

Zinc finger E-box binding homeobox 2 (ZEB2) associates with the 5'-CACCT -3' sequence in various promoters and inhibits transcription. ZEB2 has been implicated in multiple biological processes, including development, differentiation, and tumor progression. ZEB2 represses E-cadherin and causes epithelial-mesenchymal transition along with Snail and Slug (Nagaraja and Nagarajan 2018). In addition, ZEB2 activates WNT/β-catenin signaling pathways and contributes to cancer progression (Huang et al. 2020). Accumulating evidence suggests that the dysregulation of ZEB2 is involved in angiogenesis, proliferation, invasion, and metastasis of GBM. For instance, Chen et al. demonstrated that ZEB2 is an independent prognostic factor and that its overexpression is correlated with an unfavorable prognosis of GBM (Chen et al. 2018). Feng et al. reported that TRIM14 can promote the motility of GBM cells in a ZEB2-dependent manner (Feng et al. 2019). Furthermore, the MSH6-CXCR4-TGFB1 complex promotes ZEB2 transcription, leading to oncogenesis and tumor progression (Chen et al. 2019). miR-590 targets ZEB2 and ZEB1, reducing the invasiveness of GBM (Pang et al. 2015). Despite these observations, details of ZEB2-mediated signaling cascades in primary GBM are not fully understood.

MicroRNAs (miRNAs) are non-coding RNAs that contain less than 25 nucleotides. miRNAs play pivotal roles in different physical and pathological processes, including cell growth, apoptosis, and survival. Abnormal regulation of miRNAs is involved in the development of human cancer, including GBM (Saadatpour et al. 2016). Different miRNA expression profiles were used to classify the GBM sub-groups. For instance, Zeng and colleagues demonstrated that miR-17-5p and CXCL14 have potential predictive values for higher-grade gliomas (Zeng et al. 2018). In addition, an increasing number of miRNAs were identified as independent prognostic factors. A low miR-504/FZD7 expression ratio has been correlated with poor clinical outcomes against chemotherapy and radiotherapy for mesenchymal subtype GBM (Liu et al. 2019). Moreover, miRNAs can predict response to therapy. Huang et al. described the ability of miR-93 to inhibit autophagy and suggested the involvement of miR-93 in the sensitivity to therapeutic combination of irradiation and temozolomide (Huang et al. 2019). Guo et al. implicated miR-637 in a long non-coding RNA (lncRNA)- miRNA cluster that predicted the survival time of patients with wild-type BRCA1/2-subtype ovarian cancer (Guo et al. 2017). miR-637 forms a complex with various non-coding RNAs and mRNAs, and mediates oncogenesis, proliferation, chemoresistance, and metastasis. Zhang et al. demonstrated that the interplay of the lncRNA LINC00473:miR-637:CDK6 complex regulates glioma proliferation and invasion (Zhang et al. 2019b). Que et al. related the decreased miR-637 expression to shorter survival of patients with gliomas and described that overexpression of miR-637 induced tumor regression (Que et al. 2015). However, the mechanisms underlying miR-637-mediated rehabilitation remain unclear. Further investigation of miR-637 in the regulation of progression and relapse of GBM may reveal novel druggable targets.

In the present study, we observed that miR-637 was decreased in GBM. Overexpression of miR-637 reversed ZEB2-promoted cell proliferation and G1/S phase transition. Furthermore, miR-637 inhibited canonical WNT/β-catenin signaling pathways by targeting WNT7A directly. The findings reveal miR-637 as an intersection where ZEB2 and WNT/β-catenin cascades merge. The ectopic expression of miR-637 disturbed GBM progression. The novel findings will inform improvements in β-Catenin-targeted therapy of GBM.

Material And Methods

Patients and sample collection

The study was approved by the Ethics Committee of the First Hospital of China Medical University. Seventy-one patients with different grades of gliomas were recruited. All participants provided written informed consent for research purposes and publication. Independent pathologists reviewed specimen slides to validate the histological subtypes and WHO grade of gliomas (**Table 1**). The specimens were kept in liquid nitrogen.

Cell culture and establishment of ZEB2-knockdown sublines

Normal human astrocytes (NHA) were cultured in astrocyte basal medium with astrocyte growth supplements. The cells and medium were obtained from Lonza (Basel, Switzerland). The U251 and LN229 glioblastoma cell lines were purchased from the Cell Bank of the Chinese Academy of Sciences (Shanghai, China). U251 and LN229 cells were maintained in Dulbecco's modified Eagle medium (#BE12-604F, Lonza) containing 10% fetal bovine serum (F9423, Sigma-Aldrich, St. Louis, MO, USA). Short hairpin RNA targeting ZEB2 (GFP-sh-ZEB2, #TG308288), pGFP-V-RS vector (#TR30007), and Turbofectin 8.0 transfection reagent (#TF81001) were purchased from OriGene (Rockville, MD, USA). Cells were transfected with 1 μg GFP-sh-ZEB2 or pGFP-V-RS vector when the cell growth was 50-70% confluent. Stable ZEB2-knockdown clones were selected using 1 μg/ml puromycin (#P9620, Sigma-Aldrich) following the vendor's protocol. Assays were conducted 48 h post-transfection.

Plasmids and compounds

miR-637(SC400614), miR-637 anti-miRNA oligonucleotides (miR-637AMO), and pCMV-MIR vector were designed and synthesized by OriGene. The silent RNA oligo duplex targeting WNT7A was designed and synthesized by OriGene. pLKO.1 puro shRNA beta-catenin was a gift from Bob Weinberg (Addgene plasmid #18803) (Onder et al. 2008) as was pLKO.1 puro vector (Addgene plasmid #8453; http://n2t.net/addgene: 8453; RRID:Addgene_8453) (Stewart et al. 2003). Wild-type Wnt7A- (WNT7A) or mutant Wnt7A (WNT7A Mut) 3'-untranslated region (UTR) were inserted into pTA-Luc (Clontech, Mountain View, CA, USA). Tcf/Lef-luciferase was a gift from Randall Moon (Addgene plasmid #12456) (Veeman et al. 2003). Plasmids and RNA oligonucleotides were introduced into cells using Turbofectin 8.0 transfection reagent (#TF81001, OriGene) according to the manufacturer 's instructions. CCND1-luciferase was a gift from Frank McCormick (Addgene plasmid #32727) (Tetsu and McCormick 1999).

miRNA microarray analysis

miRNA and total RNA in U251 cells were extracted using the miRNeasy mini kit (#217004; Qiagen, Germany). cDNA synthesis was carried out with QuantiTect reverse transcription kit (#205311, Qiagen, Germany). miRCURY LNA miRNA Custom PCR assays (#339306, Qiagen, Germany) were used to analyze the differentially expressed miRNA between sh-NC- and sh-ZEB2 U251 sublines. The data obtained from three independent experiments were analyzed at the Gene globe data analysis center (https://geneglobe.qiagen.com/au/products/analysis-type/analysis-type-pcr/pcr-mirna/) according to the vendor's instructions. All extraction kits and analysis tools in the arrays were provided by Qiagen (Hilden, Germany). Accurate data are available in the Gene Expression Omnibus (https://www.ncbi.nlm.nih.gov/geo/query/acc.cgi?acc=GSE148779).

Analysis of miRNA and mRNA associations

The interactions between miRNA and mRNA were predicted by the miRDB database (Agarwal et al. 2015; Chen and Wang 2020) following the site instructions.

Cell proliferation assay

The 3-(4,5-dimethylthiazol-2-yl)-2,5-diphenyltetrazolium bromide (MTT) assay was performed to measure cell proliferation. Cells were seeded (1×10^4/well) in 96-well plates with 0.1 ml of medium and allowed to attach overnight. Cells were transfected with plasmids or RNA oligonucleotides according to the manufacturer' s protocols (Sigma-Aldrich, St. Louis, MO, USA). Forty-eight hours later, the cells were exposed to medium supplemented with 10 μl MTT solution (Sigma-Aldrich, #M2128; 5 mg/ml) for 4 h at 37°C. The medium was replaced by 150 μl of a solution of dimethyl sulfoxide (Sigma-Aldrich; #472301) solution, followed by incubation for 10 min. The absorbance at 490 nm was analyzed using a microplate reader (Life Science, Hercules, CA, USA).

Flow cytometry analysis

U251 cells (6×10^5) were plated in six-well petri dishes prior to analysis. Twenty-four hours later, cells were collected and fixed in 70% pre-chilled ethanol (-20°C) and incubated at 4°C overnight. Cells were resuspended gently in PBS with 50 μg/mL ribonuclease (#R6513), followed by incubation at 37°C for one h. Afterward, cells were treated with propidium iodide solution (#P4864, Sigma-Aldrich) at a final concentration of 10 μg/ml for 5 min. Cell cycle distribution was detected by flow cytometry using a FACSCalibur™ device following the manufacturer's instructions (BD Biosciences, San Jose, CA, USA). Analysis of flow cytometry data was performed using CellQuest Pro software (version 5.1; BD Biosciences). Differences among groups were estimated by two-way ANOVA, followed by a Tukey's multiple comparisons test. $P < 0.05$ was considered statistically significant. Original flow cytometry analysis data were available if required.

Luciferase reporter assay

Cells (4×10^4) per well of a 24-well plate were transfected with wild-type or mutant WNT7A 3′-UTR together with miR-637 or the vector using TurboFectin Transfection Reagent (#TF81001, OriGene). Twenty-four hours later, the luciferase signal was measured using the dual-luciferase reporter assay system (Promega, Madison, WI, USA) according to the manufacturer's protocol. Data were collected using the iMark™ Microplate Absorbance Reader (Bio-Rad) and were analyzed by two-way ANOVA followed by Sidak's multiple comparisons test. $P < 0.05$ was considered statistically significant. The relative luciferase activity is presented as values of each group normalized to the group WNT7A plus vector values.

Western blot analysis

Whole-cell protein extracts were harvested using 100 µl NP-40 lysis buffer (150 mM sodium chloride, 1.0% NP-40, 50 mM Tris, pH 8.0) with complete protease inhibitors cocktail (TaKaRa Bio/Clontech Bio Inc., Kyoto, Japan) following the manufacturer's instructions. Thirty micrograms of lysates were resolved by SDS-PAGE and transferred to nitrocellulose membranes by electroblotting. The membranes were blocked with 1% bovine serum albumin blocking buffer (#37520, Thermo Fisher Scientific, Waltham, MA, USA) for 1 h, followed by incubation with primary antibodies against ZEB2 (sc-271984), Wnt7A (sc-365665), cyclin D1 (sc-450), β-catenin (sc-7963), and glyceraldehyde 3-phosphate dehydrogenase (GAPDH, sc-0411). All antibodies were purchased from Santa Cruz Biotechnology (Dallas, TX, USA) and were used at a dilution of 1:1000 overnight at 4°C. Subsequently, the membranes were washed three times with Tris-buffered saline-Tween (TBS-T) and incubated with horseradish peroxidase-conjugated secondary antibody (TaKaRa Bio/Clontech Bio Inc.) at a dilution of 1:5000 for 1 h. Immunoreactivity was measured using Western Lighting Ultra (Thermo Fisher Scientific).

Quantitative real-time polymerase chain reaction (qRT-PCR)

Total RNA was extracted using the miRNeasy mini kit (Qiagen, Valencia, CA, USA) according to the manufacturer's protocol. Five hundred nanograms RNA was reverse transcribed to cDNA using a QuantiTect reverse transcription kit (Qiagen). Real-time PCR was performed using the Mx3000P real-time PCR system (Thermo Fisher Scientific). PCR was performed using 40 cycles of 94°C for 15 s, 60°C for 10 s, and 72°C for 20 s. All experiments were independently performed three times. Gene expression was normalized to GAPDH to analyze the relative expression using the previously described $2^{-\Delta\Delta Cq}$ method (Livak and Schmittgen 2001). The primers for detecting genes were generated by Santa Cruz Biotechnology. The sequences are: *ZEB2*, sense 5′-AATGCACAGAGTGTGGCAAGGC-3′, antisense 5′-CTGCTGATGTGCGAACTGTAGG-3′; *WNT7A*, sense 5′-AGGAGAAGGCTCACAAATGGGC-3′, antisense 5′-CGGCAATGATGGCGTAGGTGAA-3′; *CTNNB1*, sense 5'-CACAAGCAGAGTGCTGAAGGTG-3′, antisense 5'-GATTCCTGAGAGTCCAAAGACAG-3′; *GAPDH*, sense 5′-GTCTCCTCTGACTTCAACAGCG-3′, antisense 5′-ACCACCCTGTTGCTGTAGCCAA-3′; *miR-637*, sense 5'-GCTTTCGGGCTCTGCG-3′; antisense 5'-GAACATGTCTGCGTATCTC-3′; and *U6*, sense 5'-CTCGCTTCGGCAGCACAT-3'; antisense 5'-TTTGCGTGTCATCCTTGCG-3′.

U251 mouse model

The animal study was approved by the Institutional Animal Care and Use Committee of the First Hospital of China Medical University. Twenty-four 4-week-old female nude
BALB/c mice (Vital River Laboratory Animal Technology Co. Ltd., Beijing, China) were maintained under specific-pathogen-free conditions. U251 cells (5×10^6) were subcutaneously injected into the flanks of the mice. Seven days later, mice with tumors were randomized into 3 groups (n=6 per group) when the mean tumor volume approached 100 mm^3. Tumor volumes were calculated as V=0.5×L×W2, where V is the volume, L is length, and W is the width. Tumor volumes were measured every 4 days. The mice were euthanized on day 28. Tumors were removed, weighed, and recorded using standard protocols.

Immunohistochemistry staining

Tumor tissues were fixed with 10% neutral-buffered formalin (#HT501128, Sigma-Aldrich), followed by paraffin embedding. The formalin-fixed paraffin-embedded blocks were cut into 4 µm-thick sections. Sodium citrate (10 mM, pH 6.0) with 0.05 % Tween-20 (V/V) was used to retrieve antigens as previously described (Kaushal et al. 2014). Anti-Caspase-3 antibody [E87] (ab32351, Abcam) and anti-β-catenin antibody [E247] (ab32572, Abcam) were used at a dilution of 1:100 and 1:500, respectively. Mouse and rabbit specific horseradish peroxidase/ 3,3'-diaminobenzidine (ABC) Detection IHC kit (ab64264, Abcam) was used to visualize the antibody deposition. Images were captured using a model CX43 microscope (Olympus, Tokyo, Japan).

Statistical analyses

The data from all experiments are presented as means ± standard deviations. The association of gene expression was analyzed using Spearman's correlation test. Group differences were evaluated by ordinary one-way analysis of variance (ANOVA) with Dunnett's multiple comparisons test. $P < 0.05$ was statistically significant. Statistical analysis was performed using GraphPad version 8.0 (San Diego, CA, USA).

Results

ZEB2 is increased in GBM and contributes to cell proliferation and G1/S phase progression

ZEB2 expression was examined in 18 grade II, 13 grade III, and 40 grade IV (GBM) specimens. ZEB2 was increased in GBM compared to adjacent tissues, while that of grade II and III was insignificant (**Figure 1a**). There were no significant differences in ZEB2 expression among various histological subtypes of gliomas as well as gender and age (**Table 1**). Moreover, ZEB2 expression was higher at the translation and transcriptional levels in GBM cell lines than in NHA (**Figure 1b**). The findings agreed with the ZEB2 alteration in tissues. To further investigate the effect of ZEB2 on cell proliferation, we generated stable ZEB2-knockdown U251 and LN229 sublines (**Figure 1c**). The downregulation of ZEB2 impaired cell proliferation significantly compared to the sh-NC (**Figure 1d**). We selected the sh-ZEB#1 subline to analyze the cell cycle distribution because there was an insignificant difference in the growth curves of the sublines. As expected, flow cytometry analysis revealed that ZEB2-knockdown caused G1/S phase arrest (**Figure 1e**).

miR-637 suppresses cell proliferation and induces G1/S arrest in the absence of ZEB2

We conducted miRNA arrays with the sublines and control cells to investigate the alteration of the miRNA profile of ZEB2-knockdown GBM cells. The heatmaps in **Figure 2a** displayed the distinctly expressed miRNA. miR-637 showed the most considerable reduction. We also determined the expression of several miRNA candidates in sh-ZEB2 knockdown sublines (data not shown). The results were consistent with those shown in Figure 2A. We therefore explored miR-637 expression in GBM cells and tissues. The expression of miR-637 declined in GBM cells compared to that in NHA (**Figure 2b**). Moreover, miR-637 expression was significantly lower in GBM specimens than in adjacent tissues, while that of grade II and III was consistent (**Figure 2c**). The differences in miR-637 expression among histological subtypes were insignificant in chi-square analysis (**Table 1**). A negative correlation between miR-637 and ZEB2 expression was revealed by Spearman's test (**Figure 2d**). The R^2 value of 0.5605 indicated that the relationship between miR637 and ZEB2 accounted for half of the changes in miR-637 expression. The downregulation of ZEB2 promoted miR-637 (**Figure 2e**), which agreed with the results in **Figure 2d**. To determine the effects of miR-637 on cell proliferation, we introduced miR-637 mimics (miR-637), miR-637 anti-miRNA oligonucleotides (miR-637AMO), and a combination of miR-637AMO and sh-ZEB2#1 into GBM cells. The results in **Figure 2f** suggested that miR-637 expression increased in cells expressing miR-637 mimics and decreased significantly in cells expressing miR-637AMO. ZEB2 decreased markedly in cells expressing the combination. The overexpression of miR-637 suppressed cell proliferation, while the downregulation of miR-637 strikingly induced proliferation. Notably, the proliferation of ZEB2/miR637-dual knockdown cells returned to the control level (**Figure 2g**). Flow cytometry analysis showed that the percentage of the G1 phase in cells expressing miR-637 was approximately 70%, while that in cells lacking miR-637 was <40% compared to that in control cells (slightly >50%). The results suggested that the overexpression of miR-637 attenuated the G1/S phase transition, while miR-637 knockdown enhanced G1/S phase progression. The percentage of the G1 phase in cells lacking miR-637 and ZEB2 showed little change compared to the control (**Figure 2h**).

The depletion of ZEB2 enhanced miR-637 expression in GBM cells, and the ZEB2-miR637 axis was involved in the regulation of cell proliferation and G1/S transition.

miR-637 inhibits cell proliferation and G1/S phase transition by targeting WNT7A

As miRNA is involved in the regulation of tumor progression by targeting various mRNA candidates, we employed the miRDB database to predict the miRNA-mRNA interactions. Among a few candidate targets of miR-637, WNT7A expression showed the most significant augmentation in cells that lacked miR-637 (**Supplementary Figure**). WNT7A expression increased by 3.71 times in 149 glioblastoma cases than in 190 non-cancerous brain samples in the TNMplot database (https://www.tnmplot.com/), where RNA sequencing data from The Cancer Genome Atlas, Tumor Alterations Relevant for Genomics-driven Therapy, and Gene Expression Omnibus databases were analyzed using Mann-Whitney tests. Thus, WNT7A was selected for further investigation.

WNT7A was elevated in GBM cells compared with NHA (**Figure 3a**). Moreover, WNT7A expression was increased in GBM compared to adjacent tissues, whereas that in grade II and III remained consistent (**Figure 3b**). The WNT7A expression among histological subtypes was insignificantly (**Table 1**). WNT7A expression was negatively correlated with miR-637 by Spearman's rank correlation analysis (**Figure 3c**). The R^2 value of 0.5304 suggested that approximately half of the WNT7A alteration was triggered by miR-637. We generated an WNT7A mutation (WNT7A MUT) in which the scrambled nucleotides were insufficient for the binding of miR-637. The 3'-UTR of WNT7A-dependent relative luciferase activity dropped significantly, while that of WNT7A Mut only changed marginally (**Figure 3d**). The ectopic expression of miR-637AMO repressed miR-637 expression (**Figure 3e**) and promoted the expression of WNT7A (**Figure 3f**). Because WNT7A was one of the target genes of miR-637, we wondered whether miR-637 repressed cell proliferation and retarded G1/S phase transition in a WNT7A-dependent manner. Further exploration showed that the silencing of WNT7A overcame miR-637AMO-promoted cell proliferation (**Figure 3g**). In addition, the silencing of WNT7A reversed the miR-637AMO-enhanced G1/S phase progression. The results in **Figure 3h** indicated that the population of the G1 phase in cells lacked miR-637 and WNT7A returned the proportion to that of the control. The collective findings indicated that miR-637 suppressed cell proliferation and hampered G1/S transition by targeting WNT7A.

miR-637 inhibits cell proliferation and G1/S phase transition by interrupting WNT/β-catenin signaling pathways

The WNT family is essential in activating canonical WNT/β-catenin signaling cascades, including WNT7A (Noda et al. 2016). We introduced β-catenin and shRNA targeting β-cateninβ-catenin into cells in the absence of miR-637. Downregulation of miR-637 enhanced WNT7A and β-cateninβ-catenin expression, while sh-β-catenin significantly inhibited β-cateninβ-catenin expression (**Figure 4a**). Further investigation demonstrated that sh-β-catenin abolished the miR-637AMO-boosted cell proliferation (**Figure 4b**) and β-catenin abrogated miR-637AMO-induced G1/S progression (**Figure 4c**). Previous studies have established that active β-catenin binds to T-cell factor/lymphoid enhancer-binding factor (TCF/LEF) family members and triggers the transcription of target genes, such as CCND1, which encodes the critical regulator of G1/S phase transition, cyclin D1 (Shang et al. 2017). Thus, the luciferase activity of TCF/LEF binding sites is an indicator of β-Catenin-mediated transcriptional activation. We therefore introduced Tcf/Lef-luciferase or CCND1-luciferase with miR-637AMO, or a combination of miR-637AMO and sh-β-catenin into cells. As shown in **Figure 4d**, miR-637AMO significantly enhanced the luciferase activity of TCF/LEF compared to the control group, whereas the ectopic expression of sh-β-catenin defeated the miR-637AMO-mediated promotion. The changes in CCND1-luciferase were similar to those of TCF/LEF luciferase (**Figure 4e**). The results in **Figure 4** suggested that miR-637 blocked cell proliferation and cell cycle progression via WNT/β-catenin signaling pathways.

miR-637 impedes tumor growth in U251 mouse models

To illustrate the effects of miR-637 on tumor growth, we established human U251 animal models by subcutaneous injection of U251 cells. Tumor volumes of the miR-637 group declined, whereas those of miR-637AMO increased (**Figure 5a**). Notably, the tumor volume of the dual knockdown group were almost the same as those of the control group. The findings suggested that β-cateninβ-catenin knockdown abrogated miR-637AMO-enhanced tumor growth. Moreover, tumor weights in the miR-637 group decreased, while those in miR-637AMO increased in comparison with the control group. The differences in tumor weights between the dual knockdown and control groups were insignificant, consistent with the changes in growth curves (**Figure 5b**). We further examined the expression of β-catenin and caspase 3 to explore apoptosis. β-catenin was increased in the miR-637AMO group and β-catenin reduced in the miR-637 and sh-β-catenin groups compared to the control group (**Figure 5c**). In contrast, miR-637 and the dual blockage of miR-637 and β-catenin promoted caspase 3, whereas miR-637AMO repressed the expression of caspase 3 compared to the control group. The expression of WNT7A and β-catenin decreased in the miR-637 group but increased in the miR-637AMO group compared to the control group **(Figure 5d** and **e**). WNT7A expression remained consistent in the β-catenin-knockdown group compared to the miR-637AMO group, indicating that miR-637 targeted WNT7A and hampered WNT/β-catenin signaling pathways. We also determined Cyclin D1, which can be promoted by β-catenin and which promotes the G1/S phase transition (Shang et al. 2017). miR-637AMO enhanced Cyclin D1 expression, while miR-637 and the dual knockdown attenuated Cyclin D1 compared to the control group, consistent with the alteration of β-catenin (**Figure 5e**). The collective results in **Figure 5** proved that miR-637 can retard tumor growth by restricting WNT/β-catenin cascades.

Discussion

ZEB2 is characterized by two-handed zinc fingers, which associate with the 5'-CACCT-3' sequence within different promoters and repress transcription, including E-cadherin. Chen et al. demonstrated that ZEB2 overexpression resulted in a shorter overall survival of GBM patients (Chen et al. 2018). Suzuki et al. found that ZEB2 expression increased significantly in grade IV gliomas (GBM), whereas ZEB2 expression was slightly higher in grade II gliomas. ZEB2 was positively correlated with GBM invasiveness (Suzuki et al. 2018). The present results that GBM features ZEB2 overexpression, while grade II and grade III showed similar ZEB2 expression compared to non-cancerous tissues, are consistent with these previous studies.

ZEB2 cooperates with lncRNA, miRNA, and protein. The inhibition of transcription promotes GBM progression. Chen et al. showed that an oncogenic loop of MSH6-CXCR4-TGFB1 conferred GBM resistance against temozolomide in a ZEB2-dependent manner (Chen et al. 2019). Cheng et al. validated that lncRNA MALAT1 released ZEB2 from miR-124, accelerating GBM growth (Cheng et al. 2020). The details of the interplay between ZEB2 and WNT/β-Catenin remain controversial. Comijn et al. demonstrated that either the location or the expression of β-catenin was altered after SIP1 (ZEB2) induction in MDCK and SW480 cells (Comijn et al. 2001). Qi et al. argued that the knockdown of ZEB2 suppressed β-catenin expression in U251 and U87 cells (Qi et al. 2012). Zhang et al. illustrated that miR-498 targeted ZEB2 and XIAP, hindered liver cancer malignant behavior via inactivation of WNT/β-catenin pathways (Zhang et al. 2019c). Zhang and colleagues proved that the ZEB2/miR-200c loop participated in prostate carcinoma progression (Zhang et al. 2019a). We found crosstalk between ZEB2 and canonical WNT/β-catenin pathways, which are frequently activated in GBM progression, providing attractive therapeutic targets against GBM.

In the current study, we found that miR-637 expression declined in GBM, which was in agreement with previous research (Jin et al. 2020; Zhang et al. 2019b). Moreover, the present results that miR-637 presented in grade II and grade III gliomas marginally suggested that miR-637 showed potential as a predictive index for better GBM prognosis. Large samples covering different grade subtypes or diverse genetic characteristics of GBM could be helpful in the future. In addition, we found miR-637 is common to the ZEB2 and WNT/β-catenin pathways. The ectopic expression of miR-637 interrupted the collaboration of ZEB2 and β-catenin, leading to inhibited GBM growth. Chromatin immunoprecipitation coupled with high-throughput sequencing and RNA immunoprecipitation assays identified the transcriptional factors targeting miR-637 in the presence of ZEB2.

To date, few β-catenin-specific inhibitors have been evaluated in GBM-related clinical trials, although many compounds have been shown to antagonize aberrant β-catenin activity. The reasons for the discrepancy in the crosstalk between ZEB2 and β-catenin across various cancers remains unknown. Further experiments to clarify the mechanisms underlying ZEB2 repressed miR-637 are necessary. Apart from working as a tumor suppressor in GBM progression, miR-637 contributes to cancer regression in multiple cancers. Hindered miR-637 activates signal transducer and activator of transcription 3 signaling. This results in chemoresistance and tumorigenesis (Zheng et al. 2020; Zhang et al. 2019d; Zhang et al. 2011). In addition, miR-637 can inhibit Akt1 activation and prevent tumor progression (Xu et al. 2018; Leivonen et al. 2014). The present and previous findings indicate that miR-637 could be a point of convergence of ZEB2, WNT/β-Catenin, STAT3, and Akt1, which contributes to malignancy. The combination of miR-637 mimics and β-catenin inhibitors may help improve the β-catenin-targeted regimen.

Downregulation of ZEB2 can promote miR-637 expression in GBM. miR-637 overexpression suppresses the hyperactivation of WNT/β-catenin signaling cascades, hampering GBM proliferation. The crosstalk between ZEB2 and WNT/β-catenin signaling pathways can be blocked by the ectopic expression of miR-637. The findings provide new insights into the mechanisms underlying ZEB2 targeting the WNT/β-catenin pathways. The findings could inform improved β-catenin-targeted therapy for GBM.

Declarations

AUTHOR CONTRIBUTION STATEMENT

WW wrote the main manuscript. WW, ZZ, SH, and DW performed the experiments and designed the research. WW, ZZ, and DW analyzed the data. WW, SH, and DW contributed to manuscript revisions. All authors reviewed the manuscript and read and approved the final manuscript.

ACKNOWLEDGMENTS

We appreciated the gifts of plasmids from Dr. Bob Weinberg, Dr. Randall Moon, and Dr. Frank McCormick.

CONFLICT OF INTEREST STATEMENT

The authors declare that they have no conflict of interest.

DATA STATEMENT

Data obtained from the miRNA microarray analysis are available in the Gene Expression Omnibus (https://www.ncbi.nlm.nih.gov/geo/query/acc.cgi?acc=GSE148779).

FUNDING

None

References

Agarwal V, Bell GW, Nam JW, Bartel DP (2015) Predicting effective microRNA target sites in mammalian mRNAs. Elife 4. doi:10.7554/eLife.05005

Chen P, Liu H, Hou A, Sun X, Li B, Niu J, Hu L (2018) Prognostic Significance of Zinc Finger E-Box-Binding Homeobox Family in Glioblastoma. Med Sci Monit 24:1145-1151. doi:10.12659/msm.905902

Chen R, Smith-Cohn M, Cohen AL, Colman H (2017) Glioma Subclassifications and Their Clinical Significance. Neurotherapeutics 14 (2):284-297. doi:10.1007/s13311-017-0519-x

Chen Y, Liu P, Sun P, Jiang J, Zhu Y, Dong T, Cui Y, Tian Y, An T, Zhang J, Li Z, Yang X (2019) Oncogenic MSH6-CXCR4-TGFB1 Feedback Loop: A Novel Therapeutic Target of Photothermal Therapy in Glioblastoma Multiforme. Theranostics 9 (5):1453-1473. doi:10.7150/thno.29987

Chen Y, Wang X (2020) miRDB: an online database for prediction of functional microRNA targets. Nucleic Acids Res 48 (D1):D127-D131. doi:10.1093/nar/gkz757

Cheng H, Zhao H, Xiao X, Huang Q, Zeng W, Tian B, Ma T, Lu D, Jin Y, Li Y (2020) Long Non-coding RNA MALAT1 Upregulates ZEB2 Expression to Promote Malignant Progression of Glioma by Attenuating miR-124. Mol Neurobiol. doi:10.1007/s12035-020-02165-0

Comijn J, Berx G, Vermassen P, Verschueren K, van Grunsven L, Bruyneel E, Mareel M, Huylebroeck D, van Roy F (2001) The two-handed E box binding zinc finger protein SIP1 downregulates E-cadherin and induces invasion. Mol Cell 7 (6):1267-1278. doi:10.1016/s1097-2765(01)00260-x

Feng S, Cai X, Li Y, Jian X, Zhang L, Li B (2019) Tripartite motif-containing 14 (TRIM14) promotes epithelial-mesenchymal transition via ZEB2 in glioblastoma cells. J Exp Clin Cancer Res 38 (1):57. doi:10.1186/s13046-019-1070-x

Guo L, Peng Y, Meng Y, Liu Y, Yang S, Jin H, Li Q (2017) Expression profiles analysis reveals an integrated miRNA-lncRNA signature to predict survival in ovarian cancer patients with wild-type BRCA1/2. Oncotarget 8 (40):68483-68492. doi:10.18632/oncotarget.19590

He L, Zhou H, Zeng Z, Yao H, Jiang W, Qu H (2019) Wnt/beta-catenin signaling cascade: A promising target for glioma therapy. J Cell Physiol 234 (3):2217-2228. doi:10.1002/jcp.27186

Huang L, Liu Z, Hu J, Luo Z, Zhang C, Wang L, Wang Z (2020) MiR-377-3p suppresses colorectal cancer through negative regulation on Wnt/beta-catenin signaling by targeting XIAP and ZEB2. Pharmacol Res 156:104774. doi:10.1016/j.phrs.2020.104774

Huang T, Wan X, Alvarez AA, James CD, Song X, Yang Y, Sastry N, Nakano I, Sulman EP, Hu B, Cheng SY (2019) MIR93 (microRNA -93) regulates tumorigenicity and therapy response of glioblastoma by targeting autophagy. Autophagy 15 (6):1100-1111. doi:10.1080/15548627.2019.1569947

Jin C, Zhao J, Zhang ZP, Wu M, Li J, Liu B, Liao XB, Liao YX, Liu JP (2020) CircRNA EPHB4 modulates stem properties and proliferation of gliomas via sponging miR-637 and up-regulating SOX10. Mol Oncol. doi:10.1002/1878-0261.12830

Kaushal V, Herzog C, Haun RS, Kaushal GP (2014) Caspase protocols in mice. Methods Mol Biol 1133:141-154. doi:10.1007/978-1-4939-0357-3_9

Leivonen SK, Sahlberg KK, Makela R, Due EU, Kallioniemi O, Borresen-Dale AL, Perala M (2014) High-throughput screens identify microRNAs essential for HER2 positive breast cancer cell growth. Mol Oncol 8 (1):93-104. doi:10.1016/j.molonc.2013.10.001

Liu Q, Guan Y, Li Z, Wang Y, Liu Y, Cui R, Wang Y (2019) miR-504 suppresses mesenchymal phenotype of glioblastoma by directly targeting the FZD7-mediated Wnt-beta-catenin pathway. J Exp Clin Cancer Res 38 (1):358. doi:10.1186/s13046-019-1370-1

Livak KJ, Schmittgen TD (2001) Analysis of relative gene expression data using real-time quantitative PCR and the 2(-Delta Delta C(T)) Method. Methods 25 (4):402-408. doi:10.1006/meth.2001.1262

Nagaraja SS, Nagarajan D (2018) Radiation-Induced Pulmonary Epithelial-Mesenchymal Transition: A Review on Targeting Molecular Pathways and Mediators. Curr Drug Targets 19 (10):1191-1204. doi:10.2174/1389450119666180207092234

Noda M, Vallon M, Kuo CJ (2016) The Wnt7's Tale: A story of an orphan who finds her tie to a famous family. Cancer Sci 107 (5):576-582. doi:10.1111/cas.12924

Onder TT, Gupta PB, Mani SA, Yang J, Lander ES, Weinberg RA (2008) Loss of E-cadherin promotes metastasis via multiple downstream transcriptional pathways. Cancer Res 68 (10):3645-3654. doi:10.1158/0008-5472.CAN-07-2938

Pang H, Zheng Y, Zhao Y, Xiu X, Wang J (2015) miR-590-3p suppresses cancer cell migration, invasion and epithelial-mesenchymal transition in glioblastoma multiforme by targeting ZEB1 and ZEB2. Biochem Biophys Res Commun 468 (4):739-745. doi:10.1016/j.bbrc.2015.11.025

Qi S, Song Y, Peng Y, Wang H, Long H, Yu X, Li Z, Fang L, Wu A, Luo W, Zhen Y, Zhou Y, Chen Y, Mai C, Liu Z, Fang W (2012) ZEB2 mediates multiple pathways regulating cell proliferation, migration, invasion, and apoptosis in glioma. PLoS One 7 (6):e38842. doi:10.1371/journal.pone.0038842

Que T, Song Y, Liu Z, Zheng S, Long H, Li Z, Liu Y, Wang G, Liu Y, Zhou J, Zhang X, Fang W, Qi S (2015) Decreased miRNA-637 is an unfavorable prognosis marker and promotes glioma cell growth, migration and invasion via direct targeting Akt1. Oncogene 34 (38):4952-4963. doi:10.1038/onc.2014.419

Reifenberger G, Wirsching HG, Knobbe-Thomsen CB, Weller M (2017) Advances in the molecular genetics of gliomas - implications for classification and therapy. Nat Rev Clin Oncol 14 (7):434-452. doi:10.1038/nrclinonc.2016.204

Saadatpour L, Fadaee E, Fadaei S, Nassiri Mansour R, Mohammadi M, Mousavi SM, Goodarzi M, Verdi J, Mirzaei H (2016) Glioblastoma: exosome and microRNA as novel diagnosis biomarkers. Cancer Gene Ther 23 (12):415-418. doi:10.1038/cgt.2016.48

Shang S, Hua F, Hu ZW (2017) The regulation of beta-catenin activity and function in cancer: therapeutic opportunities. Oncotarget 8 (20):33972-33989. doi:10.18632/oncotarget.15687

Stewart SA, Dykxhoorn DM, Palliser D, Mizuno H, Yu EY, An DS, Sabatini DM, Chen IS, Hahn WC, Sharp PA, Weinberg RA, Novina CD (2003) Lentivirus-delivered stable gene silencing by RNAi in primary cells. RNA 9 (4):493-501. doi:10.1261/rna.2192803

Suzuki K, Kawataki T, Endo K, Miyazawa K, Kinouchi H, Saitoh M (2018) Expression of ZEBs in gliomas is associated with invasive properties and histopathological grade. Oncol Lett 16 (2):1758-1764. doi:10.3892/ol.2018.8852

Tetsu O, McCormick F (1999) Beta-catenin regulates expression of cyclin D1 in colon carcinoma cells. Nature 398 (6726):422-426. doi:10.1038/18884

Veeman MT, Slusarski DC, Kaykas A, Louie SH, Moon RT (2003) Zebrafish prickle, a modulator of noncanonical Wnt/Fz signaling, regulates gastrulation movements. Curr Biol 13 (8):680-685. doi:10.1016/s0960-9822(03)00240-9

Xu RL, He W, Tang J, Guo W, Zhuang P, Wang CQ, Fu WM, Zhang JF (2018) Primate-specific miRNA-637 inhibited tumorigenesis in human pancreatic ductal adenocarcinoma cells by suppressing Akt1 expression. Exp Cell Res 363 (2):310-314. doi:10.1016/j.yexcr.2018.01.026

Zeng A, Yin J, Wang Z, Zhang C, Li R, Zhang Z, Yan W, You Y (2018) miR-17-5p-CXCL14 axis related transcriptome profile and clinical outcome in diffuse gliomas. Oncoimmunology 7 (12):e1510277. doi:10.1080/2162402X.2018.1510277

Zhang J, Zhang H, Qin Y, Chen C, Yang J, Song N, Gu M (2019a) MicroRNA-200c-3p/ZEB2 loop plays a crucial role in the tumor progression of prostate carcinoma. Ann Transl Med 7 (7):141. doi:10.21037/atm.2019.02.40

Zhang JF, He ML, Fu WM, Wang H, Chen LZ, Zhu X, Chen Y, Xie D, Lai P, Chen G, Lu G, Lin MC, Kung HF (2011) Primate-specific microRNA-637 inhibits tumorigenesis in hepatocellular carcinoma by disrupting signal transducer and activator of transcription 3 signaling. Hepatology 54 (6):2137-2148. doi:10.1002/hep.24595

Zhang Q, Wang G, Xu L, Yao Z, Song L (2019b) Long non-coding RNA LINC00473 promotes glioma cells proliferation and invasion by impairing miR-637/CDK6 axis. Artif Cells Nanomed Biotechnol 47 (1):3896-3903. doi:10.1080/21691401.2019.1671431

Zhang X, Xu X, Ge G, Zang X, Shao M, Zou S, Zhang Y, Mao Z, Zhang J, Mao F, Qian H, Xu W (2019c) miR498 inhibits the growth and metastasis of liver cancer by targeting ZEB2. Oncol Rep 41 (3):1638-1648. doi:10.3892/or.2018.6948

Zhang Y, Li C, Liu X, Wang Y, Zhao R, Yang Y, Zheng X, Zhang Y, Zhang X (2019d) circHIPK3 promotes oxaliplatin-resistance in colorectal cancer through autophagy by sponging miR-637. EBioMedicine 48:277-288. doi:10.1016/j.ebiom.2019.09.051

Zheng X, Huang M, Xing L, Yang R, Wang X, Jiang R, Zhang L, Chen J (2020) The circRNA circSEPT9 mediated by E2F1 and EIF4A3 facilitates the carcinogenesis and development of triple-negative breast cancer. Mol Cancer 19 (1):73. doi:10.1186/s12943-020-01183-9

Table

Table 1. The clinical-pathological characters of 71 patients with glioma.

Features	Patient numbers (%)	ZEB2		*P* values	χ^2	miR-637		*P* values	χ^2	WNT7A		*P* values	χ^2
		High	Low			High	Low			High	Low		
Age													
≥ 50	59 (83.10)	36	23	0.0780	3.1068	34	25	0.5614	0.3372	35	24	0.9494	0.0040
< 50	12 (16.90)	4	8			8	4			7	5		
Gender													
Male	28 (39.43)	17	11	0.5485	0.3600	18	10	0.4779	0.5037	16	12	0.7808	0.0775
Female	43 (60.57)	23	20			24	19			26	17		
Histological type													
Astrocytoma	43 (60.57)	24	19	0.1777	3.4550	28	15	0.4164	1.7523	25	18	0.9737	0.0533
Oligodendraglioma	13 (18.31)	5	8			7	6			8	5		
Oligo-astocytoma	15 (21.12)	11	4			7	8			9	6		

*$P < 0.05$ was considered statistical significance.

Figures

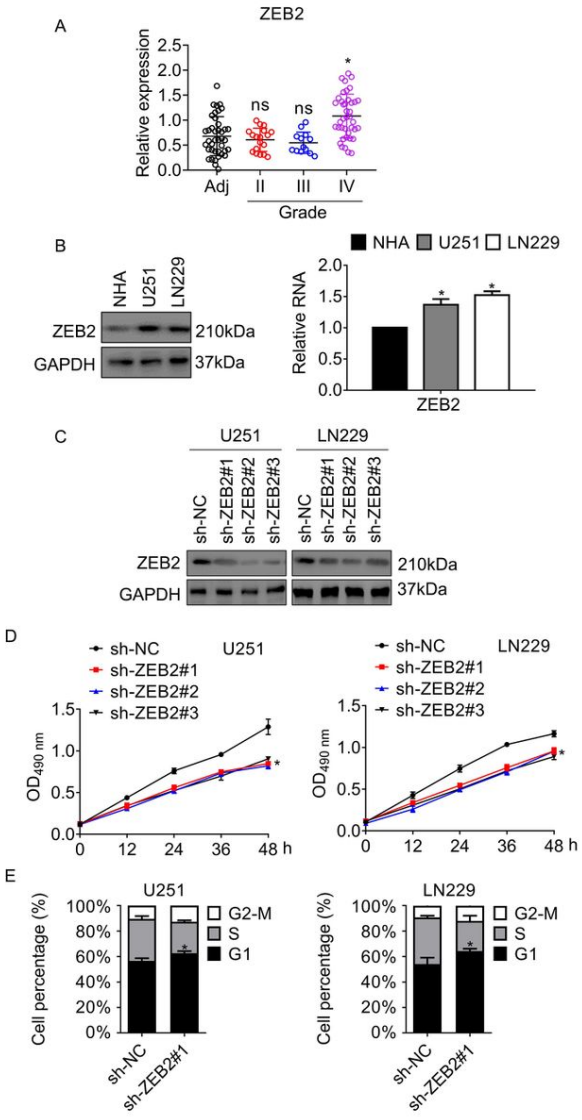

Figure 1

ZEB2 is increased in GBM and contributes to cell proliferation and G1/S phase progression. a Expression of ZEB2 in adjacent and gliomas tissues. Adj, adjacent tissues; Grade II, III, IV, WHO grade of gliomas. *P < 0.05, vs. Adj; ns, no significance, vs. Adj. b ZEB2 expression in normal human astrocytes (NHA) and GBM cell lines was detected by western blot and qRT-PCR, respectively. *P < 0.05, vs. NHA. c Depletion of ZEB2 in GBM cells validated by western blot. (D) The proliferation of the indicated cells was determined by the MTT assay. *P < 0.05, vs. sh-NC. e Cell cycle distribution of the indicated cells detected by flow cytometry. *P < 0.05, vs. sh-NC. Results represent the mean ± SD of three independent experiments. sh-NC, short hairpin RNA scrambled negative control.

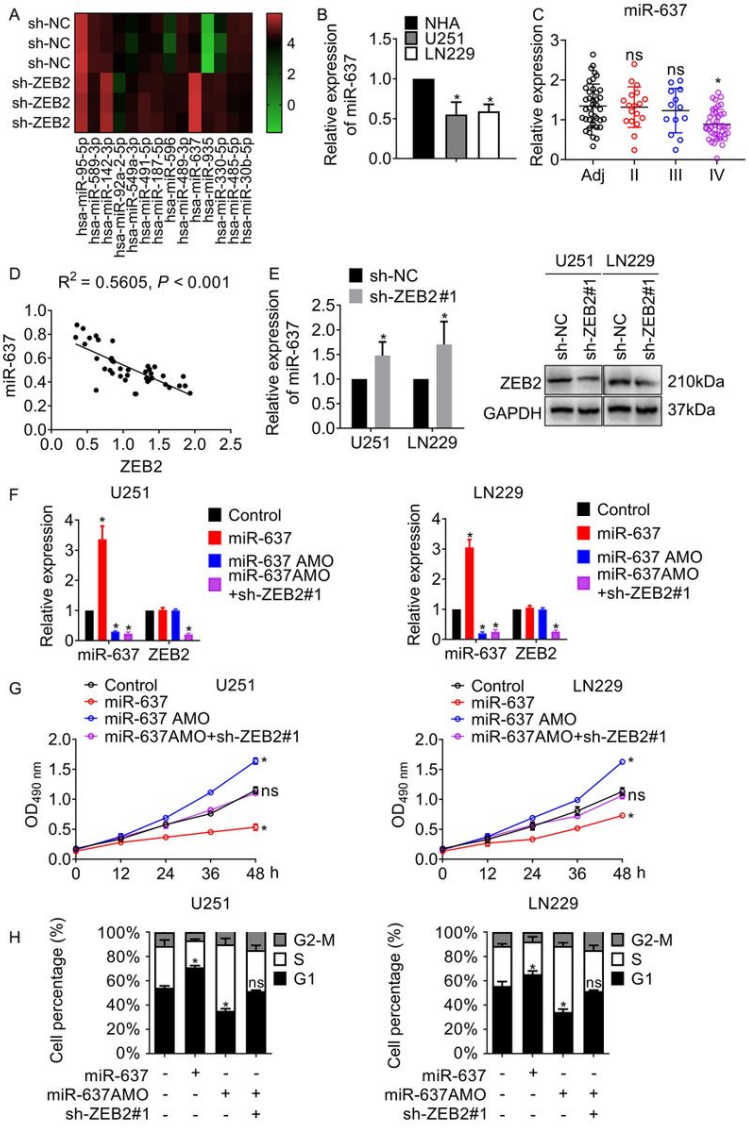

Figure 2

miR-637 is increased in ZEB2 knockdown GBM, leading to reduced cell proliferation and arrest of G1/S transition. a Differential expression of miRNAs in the indicated cells analyzed by miRNA microarray. The color indicates the fold-change of target genes compared to housekeeping genes in each group. b miR-637 expression in GBM cell lines was examined by qRT-PCR. *P < 0.05, vs. NHA. c miR-637 expression in adjacent or glioma tissues examined by qRT-PCR. *P < 0.05, vs. Adj; ns, no significance, vs. Adj. d Correlation of ZEB2 and miR-637 expression estimated by the Spearman correlation test. P < 0.05 indicated statistical significance. e Expression of miR-637 in the indicated cells analyzed by qRT-PCR. *P < 0.05, vs. sh-NC. f Expression of miR-637 and ZEB2 in the indicated cells detected by qRT-PCR. *P < 0.05, vs. Control. g Proliferation determined by MTT assay. *P < 0.05, vs. Control. h Cell cycle distribution analyzed by flow cytometry. *P < 0.05, vs. Control. Results represent the mean ± SD of three independent experiments.

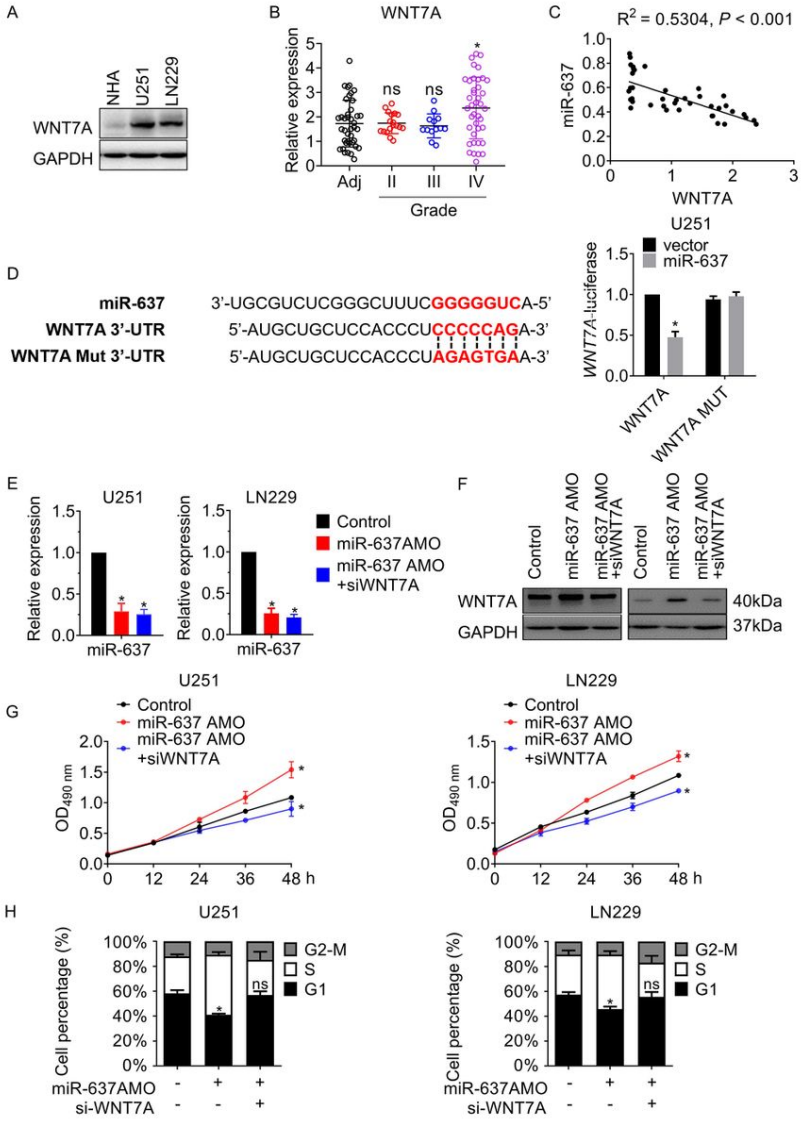

Figure 3

miR-637 inhibits cell proliferation and cell cycle progression by targeting WNT7A. a WNT7A expression in glioma cell lines examined by qRT-PCR. *P < 0.05, vs. NHA. b WNT7A expression in adjacent or gliomas tissues examined by qRT-PCR. Adj, adjacent tissues; Grade II, III, IV, WHO grade of gliomas. *P < 0.05, vs. Adj; ns, no significance, vs. Adj. c Correlation of WNT7A and miR-637 estimated by Spearman correlation analysis. P < 0.05 indicated statistical significance. d Schematic of the binding sites between ZEB2 and miR-637 and the relative luciferase activity of WNT7A determined by dual-luciferase assay. *P < 0.05, vs. vector. e Expression of miR-637 in cells analyzed by qRT-PCR. *P < 0.05, vs. Control. f Expression of WNT7A in cells analyzed by western blot. g Proliferation of the indicated cells determined by the MTT assay. *P < 0.05, vs. Control. h Cell cycle distribution of the indicated cells analyzed by flow cytometry. *P < 0.05, vs. Control. Results represent the mean ± SD of three independent experiments.

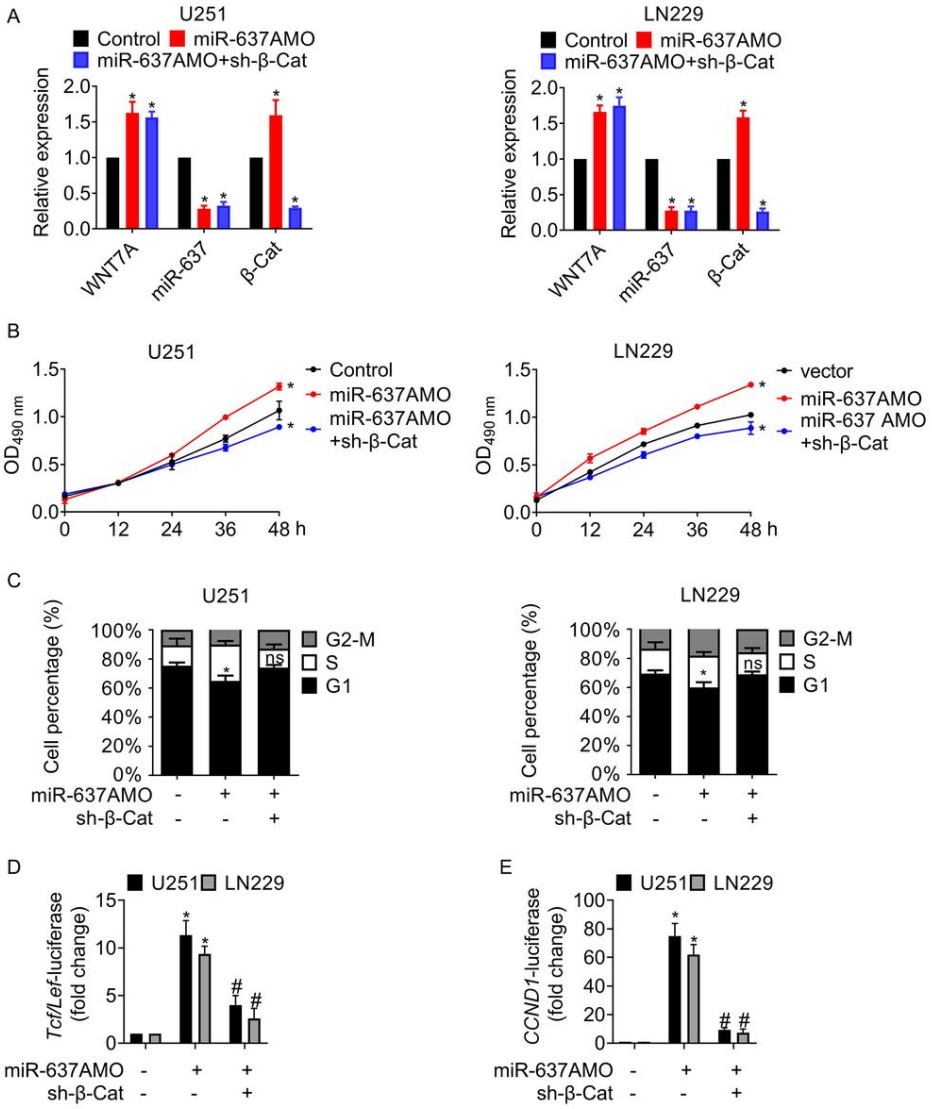

Figure 4

miR-637 suppresses proliferation and induces G1/S phase arrest by interrupting WNT/β-catenin signaling. a Gene expression determined by qRT-PCR. *P < 0.05, vs. Control. *P < 0.05, vs. Control. b Proliferation determined by the MTT assay. *P < 0.05, vs. Control. c Cell cycle distribution analyzed by flow cytometry. *P < 0.05, vs. Control; ns, vs. Control. ns, no significance. d, e Relative luciferase activity of TCF/LEF or CCND1 assessed by the dual-luciferase reporter system. * P < 0.05, vs. Control. # P < 0.05, vs. Mir-637AMO. sh-β-Cat, shRNA targeting β-catenin.

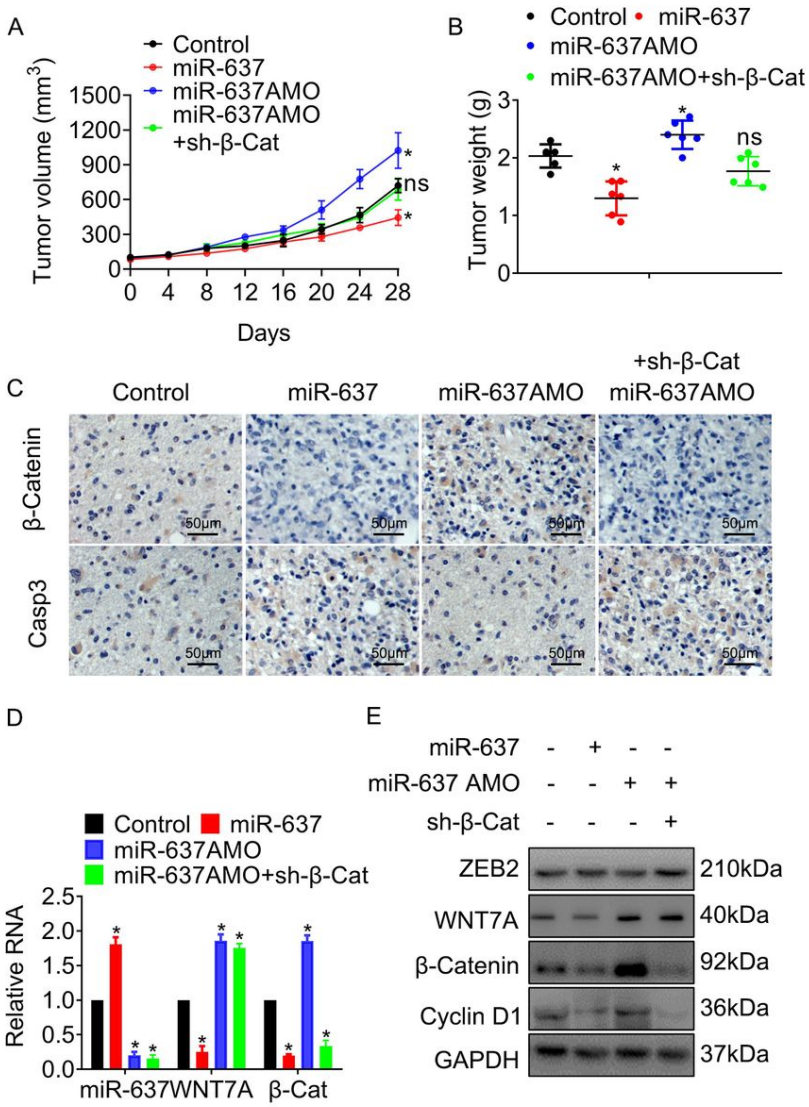

Figure 5

miR-637 hinders tumor growth in U251 xenograft models. a Tumor growth curves recorded during treatment. *P < 0.05, vs. Control; ns, vs. Control. ns, no significance. b Tumor weights measured post-treatment. *P < 0.05, vs. Control; ns, vs. Control. ns, no significance. c Gene expression determined using immunohistochemistry. Magnification, 400×. d Gene expression determined by qRT-PCR. *P < 0.05, vs. Control. e Gene expression determined by western blot. Results represent the mean ± SD of three independent experiments.

Supplementary Files

This is a list of supplementary files associated with this preprint. Click to download.

- Figuresupp.jpg